International Journal of Luminescence and applications
Vol6 (4) January, 2017, **ISSN 2277 – 6362**

Structural and Luminescent properties of undoped and tungsten doped $Zn_3(PO_4)_2ZnO$ Nanocomposites

K. Satyavathi, M. Subba Rao, Sandhya Cole*

Department of Physics, Acharya Nagarjuna University, Nagarjuna Nagar, Guntur - 522 510, India
**Corresponding author Tel.: +91 863 2346383 (Lab.), mobile: +91 9441902295.*
E-mail address: sandhya.cole@gmail.com

Abstract *- Pure and tungsten doped $Zn_3(PO_4)_2ZnO$ nanocomposites (NCs) have been successfully synthesized by Sol-gel method at room temperature. The NCs have been characterized by a number of systematic investigations like X-ray Diffraction (XRD), Fourier Transform Infrared (FT-IR) spectroscopy and Photoluminescence (PL) spectroscopy techniques for different mol% concentrations of WO_3. XRD pattern reveals that the prepared samples are in crystalline nature in which $Zn_3(PO_4)_2$ corresponding to monoclinic phase and ZnO corresponding to hexagonal wurtzite phase, the average crystallite size of prepared nanopowders is in the range of 20-30nm. The lattice strain, lattice cell parameters, unit cell volume and dislocation density of the prepared nanocomposites are also calculated. IR spectra of prepared samples exhibit the characteristic sharp absorption band peaks. The sharp absorption bands observed in the region 1200-900 cm^{-1} are due to complex stretching of characteristic PO_4^{3-} groups. The PL spectra exhibit four emission peaks in the visible region indicate the quantum-confinement-induced photoluminescence and the strong emission peak of blue region also indicate the good optical quality with less defect states of the prepared samples. The CIE chromaticity diagram suggests that the prepared nanocrystalline phosphors have good color purity.*

Keywords: *Tungsten ions, XRD, FT-IR, PL spectroscopy techniques.*

1. INTRODUCTION

Inorganic nanostructures are becoming ideal systems for relieving a new phenomenon at nano scale leading towards wide range of applications. From few past decades, the use of semiconductor nanomaterials has expanded tremendously owing to their novel optical, electrical and catalytic properties. Due to their variety of applications, phosphate materials are receiving much attraction in optical, electrical, and structural fields as fluorescent materials, dielectric substances, dental cements, metal surface coatings, fuel cells, pigments [1-3]. Zinc phosphate ($Zn_3(PO_4)_2$) is a white inorganic non-toxic semiconductor featuring corrosion protection and adhesion capability. It is used as a flame retardant and also as a chemically bonded ceramic (CBC) material [4, 5]. Different phosphors are used in the color televisions for their emission in frequency ranges corresponding to each of the primary colors and the decay time of the phosphor is vital in these applications, with the relevant time scale imposed for the electron beam to sweep the phase of the tube. Zinc oxide (ZnO) is one of the important n-type inorganic multifunctional semiconductors which provide the study of nanoscale for exploring dependence of material properties on their size, shape and dimensionality. ZnO is a wide band gap (3.37eV) and large exciton binding energy (60meV) metal oxide semiconductor, which has been extensively studied due to its intrinsic properties and potential applications, used in field-effect transistors, resonators, gas sensors, solar cells and as a catalyst [6].

The effect of dopants on optical properties of $Zn_3(PO_4)_2ZnO$ NCs is very important for photonic applications. One particular dopant that can be induced several interesting properties in $Zn_3(PO_4)_2ZnO$ nanostructure is tungsten trioxide (WO_3). Tungsten has the oxidation state (+VI) and its density is higher than Cr and Mo which are found in its group. It possesses different valance states such as W^{6+}, W^{5+} and also in W^{4+} state. Due to its outstanding electronic, electro chromic [7], gas sensor [8], catalytic [9] and photoluminescence properties [10], tungsten trioxide has been used to develop smart window, anti-glare rear view mirrors of automobiles, optical recording devices, solid-state gas sensing and biosensors [11] etc. Especially, it has been also found that the gas-sensing properties (e.g., sensitivity, response-recovery, reproducibility and stability) of $Zn_3(PO_4)_2ZnO$ NCs doped with WO_3 are substantially improved by reducing the grain size to

nanoscale dimensions due to the nano-size effects leading to high density of surface active sites and large surface-to-volume ratios in comparison with their bulk counterparts [12]. The possible reason for doping $Zn_3(PO_4)_2ZnO$ with WO_3 is that W^{6+} can easily enter into the crystal lattice of $Zn_3(PO_4)_2ZnO$ due to similar ionic radius of W^{6+} and Zn^{2+}.

Several methods are used to prepare nanomaterials such as sol-gel, acidification method, chemical co precipitation method and hydrothermal method etc., out of these, sol-gel is an inexpensive, low temp and research oriented technique. This method has the main advantage of good stoichiometric control and the production of ultra fine particles with high purity in a relatively short processing time at lower temperatures with improved compositional homogeneity. Thus the aim of present is to study the structural and luminescent properties of the undoped $Zn_3(PO_4)_2ZnO$ and WO_3-doped $Zn_3(PO_4)_2ZnO$ NCs prepared by sol-gel method using powder X-ray Diffraction (XRD), Fourier Transform Infrared (FT-IR) spectroscopy and Photo Luminescence (PL) with CIE-diagram spectroscopy techniques respectively.

2. EXPERIMENTAL

2.1 Composite Preparation

The synthesis of undoped $Zn_3(PO_4)_2ZnO$ and $Zn_3(PO_4)_2ZnO$:WO_3 doped NCs are prepared by sol-gel route. The Zinc phosphate ($Zn_3(PO_4)_2$:99.9%), Zinc oxide (ZnO:99.9%) and Tungsten oxide (WO_3:99.9%) are the starting materials and weighed according to the desired stoichiometric ratio. They are dissolved in 200ml of ethanol in a beaker and the resulting solution is continuously stirred with the help of a magnetic stirrer at room temperature. During the process, 20gm of sodium hydroxide solution is dissolved in 100ml of distilled water in another beaker; 16ml of prepared NaOH solution is added drop wise to the prepared solution under constant stirring touching the walls of the beaker to get an aqueous solution. This aqueous solution now turns into a white colloid without any precipitation. The process is allowed to continue for four hours and the solution is allowed to settle. The precipitates are collected through centrifugation process, washed three times with distilled water and are dried at 200ºC for two hours inside an annealing chamber operated at ambient pressure. Thus the undoped and WO_3-doped (0.2 mol%, 0.4 mol% and 0.6 mol%) $Zn_3(PO_4)_2ZnO$ NCs are prepared.

2.2 Characterization techniques

The phase compositions of the undoped and WO_3-doped $Zn_3(PO_4)_2ZnO$ nanocomposites are characterized by XRD-6100 SHIMADZU X-Ray diffractometer in the scanning range of 10^o - 80^o (2θ) using CuK_α radiation having a wavelength of 1.5406 Å, the operation voltage and current are maintained at 40 KV and 30 mA with a scanning speed of 2 degree/min. The infrared transmission spectra of the synthesized nanocomposites are measured at room temperature in the wave number range 400–4000 cm^{-1} by a Fourier transform computerized infra-red spectrometer type (SHIMADZU-IR Affinity-1S FT-IR spectrophotometer). The PL spectrum is recorded in a PERKIN ELMER LS-55 with a Xenon lamp of excitation 325 nm.

3. RESULTS AND DISCUSSION

3.1 Phase and Element analysis

A typical XRD pattern of the prepared nanocomposites is as shown in **Fig. 1** and sharp peak intensities indicate crystalline nature of the prepared samples. From the XRD pattern, line broadening clearly indicates synthesized composites are in nanoscale. The strong peaks obtained in the all prepared nanocrystalline powders at 2θ values ≈ 12.13°, 19.25°, 21.07°, 22.45°, 24.58°, 28.30°, 28.97°, 31.74°, 34.37°, 37.15°, 39.18°, 40.50°, 42.50°, 43.36°, 44.96°, 46.56°, 51.09°, 59.63°, 61.30° and 64.36° corresponds to the lattice planes (200), (011), (111), (002), (-311), (202),(-411), (020), (600), (022), (420), (213), (-422), (611), (-613), (711), (-224), (-415), (-515) and (115) respectively confirm that the prepared samples are good crystalline in nature with monoclinic structure of zinc phosphate $Zn_3(PO_4)_2$ which is matched with the standard XRD data of JCPDS card number: 29-1390 and 36.20°, 47.47°, 56.66°, 62.80°, 65.89°, 67.88° and 69.05° corresponds to (100), (002), (101), (102), (200), (112) and (201) lattice planes respectively are indexed to typical hexagonal wurtzite structure of ZnO with JCPDS card number: 36-1451.

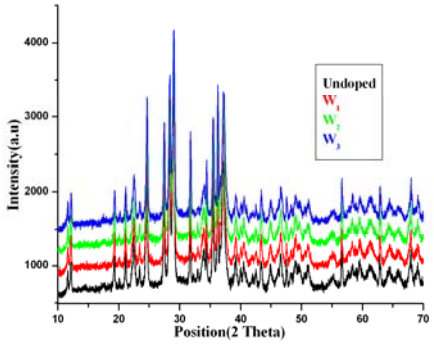

Fig. 1: XRD pattern for undoped and WO_3 doped $Zn_3(PO_4)_2ZnO$ NCs

The mean crystallite size (D) can be evaluated from the full width at half maximum (FWHM) of the diffraction peaks. According to Debye - Scherrer's equation [13], the crystallite size is given by,

$$D = \frac{0.89\lambda}{\beta cos\theta} \quad (1)$$

The lattice strain (ε) is also calculated for the same diffraction lines using Stokes and Wilson equation [14], which is given by

$$\varepsilon = \frac{\beta}{4\tan\theta} \quad (2)$$

The dislocation density (δ) is estimated from the crystalline size [15] and is given by

$\delta = 1/D^2$ (3)

Here, D is the mean grain size, λ is the X-ray wavelength (1.5406Å), β is the full width of half maximum (FWHM) in radians of the X-ray intensity of diffraction line and θ is the Bragg's diffraction angle.

There is no peak for the formation of metal oxide such as WO_3-doped $Zn_3(PO_4)_2ZnO$ NCs and the very slight change in the position of the diffraction peaks between undoped and WO_3-doped $Zn_3(PO_4)_2ZnO$ NCs indicate that some of W^{6+} ions entered into the crystal lattice of $Zn_3(PO_4)_2ZnO$ because the radius of W^{6+} ion (0.068 nm) is similar to the radius of Zn^{2+} ion (0.074 nm) which create more oxygen vacancies for charge compensation and improve the photocatalytic performance of $Zn_3(PO_4)_2ZnO$. The slight changes in lattice parameters also confirms that the substitution of tungsten ions in the $Zn_3(PO_4)_2ZnO$ lattice site. **Table 1** and **2** give the crystallite size, lattice strain, dislocation density, lattice cell parameters, unit cell volume and axes of symmetry of undoped and WO_3-doped $Zn_3(PO_4)_2ZnO$ nanopowders respectively.

3.2 Fourier transforms infrared spectroscopy (FT-IR)

FT-IR spectra of undoped and WO_3-doped $Zn_3(PO_4)_2ZnO$ nanocrystalline powders are recorded at room temperature in the middle IR region of 4000 to 400 cm^{-1} as shown in **Fig. 2**. The sharp absorption bands observed in the region 1200-900 cm^{-1} are due to complex stretching of characteristic PO_4^{3-} groups [16].

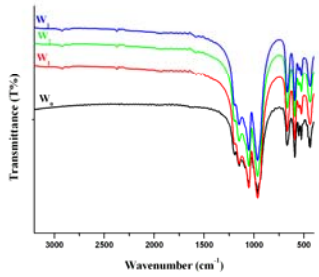

Fig. 2: FT-IR Spectra for undoped and WO_3 - doped $Zn_3(PO_4)_2ZnO$ NCs

The peak in the range of 420-450 cm^{-1} can be associated to the stretching vibration mode of the Zn-O [17]. The bands observed around at 1157 cm^{-1} are assigned to symmetric stretching of PO_4^{3-} group. The band located at 1056 cm^{-1} is due to anti-symmetric stretching of PO_4^{3-} group. The bands appeared at around 966 cm^{-1} are attributed to asymmetric P-O stretching mode and the bands observed at 672 cm^{-1} are assigned to symmetric P-O stretching mode. The bands observed around at 598 cm^{-1} are due to asymmetric O-P-O vibrational mode and the bands observed at 561 cm^{-1} are assigned to symmetric O-P-O vibrational mode [18]. In addition to the above bands, another two bands are observed, one is about 530 cm^{-1} is identified due to Zn-O tetrahedral units and the other around 445 cm^{-1} is identified due to Zn-O. The position of bands slightly shifts towards smaller wavenumber with the increasing content of WO_3. Hence the stretching of PO_4^{3-} group is a longer wavelength shift i.e., a red shift.

3.3 Photoluminescence (PL) studies

PL spectra of the WO_3-doped $Zn_3(PO_4)_2ZnO$ nanocomposites measured using an Xenon laser of 325 nm as excitation source at room temperature is as shown in **Fig. 3**. In the present study, UV emission is absent as the excitation energy is considerably lower than its band gap energy and hence only visible bands (deep level emission, DLE) are appeared, which are caused by impurities and structure defects [19]. The PL spectra of pure and WO_3-doped $Zn_3(PO_4)_2ZnO$ NCs exhibit four emission peaks with similar curve shapes in visible region: a strong blue emission at ~ 462 nm (2.915 eV), a green-yellow emission at ~ 536 nm (2.317 eV), a weak orange band at 616 nm (2.016 eV) and a weak red band at 674 nm(1.843eV).

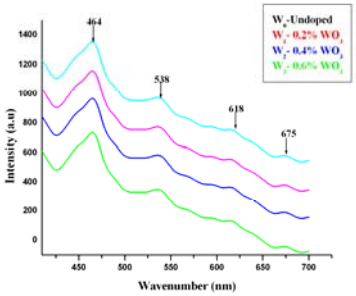

Fig. 3: PL spectra of undoped and WO_3-doped $Zn_3(PO_4)_2$ZnONCs

Because of the large surface-to-volume ratio of WO_3-doped $Zn_3(PO_4)_2$ZnO particles shows efficient and fast trapping of photo-generated holes at surface sites.

Table 1: Average crystallite size, strain and dislocation density variations of undoped and WO_3 doped $Zn_3(PO_4)_2ZnO$ NCs

Sample Code	Lattice Size (D) (nm)	Lattice strain [(ε)x10^{-4}]	Dislocation density(δ) (lines/m^2)x10^{15}
W_0	21.76	63.65	2.11
W_1	22.98	60.25	1.89
W_2	24.81	55.83	1.62
W_3	25.22	54.91	1.57

Table 2: Lattice cell parameters (2a & 2b), unit cell volume and axes of symmetry for undoped and WO_3 doped $Zn_3(PO_4)_2$ NCs

Table 2a:

Sample Code	$Zn_3(PO_4)_2$				
	Lattice Cell Parameters (Å)			Unit Cell Volume (Å)^3	Axes of Symmetry
	a	b	c	V	α = γ=90° and β
W_0	15.00	5.60	8.17	665.31	104.83°
W_1	15.01	5.60	8.19	668.39	104.98°
W_2	15.03	5.61	8.20	668.42	105.01°
W_3	15.04	5.61	8.21	669.10	105.14°

Table 2b:

Sample Code	ZnO			
	Lattice Cell Parameters (Å)		Unit Cell Volume (Å)^3	Axes of Symmetry
	a=b	c	V	α=β=90° and γ
W_0	3.25	5.25	47.80	120°
W_1	3.25	5.25	47.81	120°
W_2	3.25	5.25	47.82	120°
W_3	3.25	5.25	47.82	120°

The peak at 462 nm is ascribed to zinc vacancy (V_{Zn}), the peak at 536 nm is assigned to oxygen antisite (O_{Zn}); the peaks at 616 nm and 674 nm are attributed to oxygen interstitial (O_i) and oxygen vacancy (V_O) [21-24] respectively. Strong blue emission band at 462 nm (2.915 eV) is associated with Zn vacancies [25] due to surface defects indicates better crystal quality and good optical properties because surface states are very important for the physical properties especially for the optical properties of nanomaterials and the strong emission intensity should be attributed to the high purity with perfect crystallinity of the synthesized nanopowder. This characteristic feature may represent the possible applications in white LEDs and display devices. The green-yellow emission corresponds to the singly ionized oxygen vacancy in $Zn_3(PO_4)_2ZnO$ and this emission results from the recombination of a photogenerated hole with the singly ionized charge state of the specific defect [26]. The low intensity of the green-yellow emission is due to the low density of oxygen vacancies during the preparation of the WO_3-doped $Zn_3(PO_4)_2ZnO$ NCs.

From the solid state physics, Zn_i and V_O are electron donors and V_{Zn}, O_i and O_{Zn} are electron acceptors [27]. The peak at 666.4 nm is related to electron donors, the peaks at 471.3, 522.3 and 616.5 nm are related to electron acceptors and the gas sensitivity is significantly improved with the increase in electron donor defects because much

more oxygens are able to be chemisorbed and ionized on the surface of metal oxide semiconductors (MOS). Therefore in the present study, $Zn_3(PO_4)_2ZnO$ nanocomposite doped with WO_3 is considerer to be a promising candidate in fabrication of high performance gas sensors.

The CCT values of undoped and WO_3-doped $Zn_3(PO_4)_2ZnO$ nanocomposites lies in between 9644-7673 K respectively. Generally, CCT value greater than 5000 K indicates the cold white light used for commercial lighting purpose and less than 5000 K indicates the warm white light used for home appliances. Hence, $Zn_3(PO_4)_2ZnO$ nanocomposite emits a near cold white light emission and is useful for White Light Emitting Diodes (W-LEDs), electroluminescence panels and Plasma Display Panels (PDPs) .

CONCLUSION

Undoped and WO_3 doped $Zn_3(PO_4)_2ZnO$ nanocomposites are synthesized by sol-gel route, is an environmentally safe method. XRD pattern of prepared NCs confirm the monoclinic structure of $Zn_3(PO_4)_2$ and hexagonal structure of ZnO. From IR spectra, the existence of phosphate (PO_4^{3-}) groups and Zn-O bands confirm the formation of $Zn_3(PO_4)_2ZnO$ NCs. From PL spectra, strong emission peak in blue region indicates high structural and optical quality.

ACKNOWLEDGEMENTS

One of the authors would like to thank the **UGC-BSR Fellowship** for granting the Meritorious Research Fellowship **(Letter No. F. 25-1/2014-15). DST-FIST and DRS**, New Delhi sanctioning the equipments to the Department of Physics, ANU. The authors also thankful to the **Centralized Laboratory**, Acharya Nagarjuna University for providing Ultracentrifuge facility to carry out the present work.

REFERENCES

[1] M.A. Lopez-Quintela, J. Rivas, J. Colloid Interface Sci.158 (1993) 446.
[2] H. Nariai, S. Shibamoto, H. Maki, I. Motooka, Phosphorus Res. Bull. 8 (1998) 101
[3] H. Onoda, H. Nariai, H. Maki, I. Motooka, Phosphorus Res. Bull. 9 (1999) 69
[4] J.E. Marion, M.J. Weber, Eur. J. Solid State Inorg. Chem.28 (1991) 271
[5] H. Engqvist, J.E.S. Walz, J. Loof, G.A.Botton, D. Mayer, M.W. Phaneul, N.O.Ahnfelt, L. Hermansson, Biomaterials 25 (2004) 2781.
[6] N. Jayadevdayan, R.N. Karekar, R.C. Aiyer, S.R. Sainkar, J. Mater. Sci. Mater. Electron. 8 (1997) 277.
[7] D.S. Lee, D.D. Lee, H.R. Hwang, J.H. Paik, J.S. Huh, J.O. Lim, J.J. Lee, J. Mater. Sci. Mater. Electron. 12 (2001) 41.
[8] E. Gyorgy, G. Socol, I.N. Mihailescu, C. Ducu, S. Ciuca, J. Appl. Phys. 97 (2005) 093527.
[9] M.A. Gondal, A. Hameed, Z.H. Yamani, A. Suwaiyan, Chem. Phys. Lett. 385 (2004) 111
[10] M. Feng, A.L. Pan, H.R. Zhang, Z.A. Li, F. Liu, H.W. Liu, D.X. Shi, B.S. Zou, H.J. Gao, J. Appl. Phys. Lett. 86 (2005) 141901
[11] S.J. Ippolito, S. Kandasamy, K. Kalanatar-zadeh, W. Wlodarski, Sensor and Actuators B: Chemical 108 (2006) 154.
[12] L.A. Patil, M.D. Shinde, A.R. Bari, V.V. Deo, Sens. Actuators B 143 (2009) 270.
[13] C.S. Tiwary, R. Sarkar, P. Kumbhar, A.K. Mitra, Phys. Lett. A 372 (2008) 5825
[14] A.R. Stokes, A.J.C. Wilson, Proceeding of the Physical Society, 56 (1944) 174
[15] G.Tirumala Rao, B. Babu, R. Jouce Stella, V. Pushpa Manjari, R.V.S.S.N. Ravikumar, Spectrochimica Acta Part A 139 (2015) 86.
[16] M. Zhang, J. K. Liu, R. Miao, G. M. Li, Y. J. Du, Nano-scale Research Letters 5 (2010) 675.
[17] M. Subba Rao, K. Satyavathi, Y. Naga Bhaskararao, Sandhya Cole, J. Alloys Compd. 682 (2016) 7
[18] Y. Liu, W. Wang, Y. Zhan, G. Wang, Mater. Lett. 56 (2002) 496
[19] N.Y. Garces, L. Wang, L. Bai, N.C. Giles, L.E. Halliburton, G. Cantwell, Appl. Phys. Lett. 81 (2002) 622
[20] R. Krithiga, G. Chandrasekaran, J. Cryst. Growth 311 (2009) 4610
[21] K.T. Roro, J.K. Dangbegnon, S. Sivaraya, A.W.R. Leitch, J.R. Botha, J. Appl. Phys. 103 (2008) 053516.
[22] C.H. Tsai, W.C. Wang, F.L. Jenq, C.C. Liu, C.I. Hung, M.P. Houng, J. Appl. Phys. 104 (2008) 053521
[23] X.L. Wu, G.G. Siu, C.L. Fu, H.C. Ong, Appl. Phys. Lett. 78 (2001) 2285
[24] Z. Fan, P. Chang, J.G. Lu, E.C. Walter, R.M. Penner, C. Lin, H.P. Lee, Appl. Phys. Lett. 8 (2004) 6128
[25] H. Zeng, W. Cai, J. Hu, G. Duan, P. Liu, Y. Li, Appl. Phys. Lett. 88 (2006) 171910
[26] C.T. Hsieh, J.M. Chen, H.H. Lin, C.H. Shih, "Appl. Phys. Lett. 83 (2003) 3383
[27] F. Tuomisto, K. Saarinen, D.C. Look, G.C. Farlow, Phys. Rev. B 72 (2005) 85206.